ELSEVIER

Computer-Aided Design 37 (2005) 693–709

COMPUTER-AIDED DESIGN

www.elsevier.com/locate/cad

Subdivision surfaces for CAD—an overview

Weiyin Ma*

Department of Manufacturing Engineering and Engineering Management, City University of Hong Kong, 83 Tat Chee Avenue, Kowloon, Hong Kong, China

Received 16 August 2004

Abstract

Subdivision surfaces refer to a class of modelling schemes that define an object through recursive subdivision starting from an initial control mesh. Similar to B-splines, the final surface is defined by the vertices of the initial control mesh. These surfaces were initially conceived as an extension of splines in modelling objects with a control mesh of arbitrary topology. They exhibit a number of advantages over traditional splines. Today one can find a variety of subdivision schemes for geometric design and graphics applications. This paper provides an overview of subdivision surfaces with a particular emphasis on schemes generalizing splines. Some common issues on subdivision surface modelling are addressed. Several key topics, such as scheme construction, property analysis, parametric evaluation and subdivision surface fitting, are discussed. Some other important topics are also summarized for potential future research and development. Several examples are provided to highlight the modelling capability of subdivision surfaces for CAD applications.

Keywords: B-splines; Subdivision surfaces; Arbitrary topology; Limit surface

1. Introduction

In the field of computer-aided design (CAD) and related industries, the de-facto standard for shape modelling is at present non-uniform rational B-splines (NURBS). NURBS representation, however, uses a rigid rectangular grid of control points and has limitations in manipulating shapes of general topology. Subdivision surfaces provide a promising complimentary solution to NURBS. It allows the design of efficient, hierarchical, local, and adaptive algorithms for modelling, rendering and manipulating free-form objects of arbitrary topology.

In connection with shape representation, subdivision-based modeling can be dated back to Chaikin's corner cutting algorithm for defining free-form curves starting from an initial control polygon through recursive refinement [7]. In the limit, Chaikin's algorithm produces uniform quadratic B-spline curves. The scheme was later extended by Doo and Sabin [10] and Catmull and Clark [6] for defining free-form surfaces starting from an initial control mesh of arbitrary topology. For a set of regular rectangular control points, Doo–Sabin subdivision produces uniform bi-quadratic B-spline surfaces and Catmull–Clark subdivision produces uniform bi-cubic B-spline surfaces. They are therefore extensions of uniform bi-quadratic and bi-cubic B-spline surfaces, respectively, for control meshes of arbitrary topology type. In addition one can also define various sharp features, such as crease edges, corners and darts. Today, one may find rich families of subdivision surfaces (such as classical schemes [6,10,11,14,18–20,22,23,27,37,54,60], and unified and combined schemes [35,47,50,51,55,57,62]) widely used in geometric design and computer graphics for shape design, animation, multi-resolution modelling and many other engineering applications [9,42,43,56,61]. Subdivision surfaces possess various important properties similar to B-splines. In addition, the extension to arbitrary topology and sharp features makes subdivision surfaces a valuable asset in complimentary to NURBS.

This paper provides an introduction to subdivision surfaces with a particular emphasis on schemes that generalize B-spline surfaces.

* Tel.: +852 2788 9548; fax: +852 2788 8423.
E-mail address: mewma@cityu.edu.hk

0010-4485//$ - see front matter © 2004 Elsevier Ltd. All rights reserved.
doi:10.1016/j.cad.2004.08.008

2. The basic idea of subdivision

The basic idea of subdivision is to define a smooth surface as the limit surface of a subdivision process in which an initial control mesh is repeatedly refined with newly inserted vertices. In this section, we introduce two subdivision schemes, i.e. the Chaikin's algorithm for curve refinement and Doo–Sabin subdivision for surface modeling. Section 3 further introduces how this kind of schemes can be developed from the spline theory.

2.1. Chaikin's algorithm for curve subdivision

Fig. 1 shows a closed curve refined through corner cutting using Chaikin's algorithm. Each of the control vertices of a refined mesh is computed as an affine combination of old neighboring vertices. In the limit, the refined mesh converges to a smooth curve which is known as an uniform quadratic B-spline curve.

Chaikin's subdivision has two essential components common to all subdivision schemes, i.e. topological rules and geometric rules.

- The topological rules of Chaikin's subdivision are shown in Fig. 2, which is often called corner cutting. For each old vertex v_i, the corner is cut off by inserting two new vertices v'_{2i} and v'_{2i+1} and is replaced by a new edge $v'_{2i}v'_{2i+1}$ connecting the two newly inserted vertices. The length of all old edges are thus reduced, e.g. to $v'_{2i+1}v'_{2i+2}$ for old edge v_iv_{i+1}.
- The geometric rules for Chaikin's algorithm are defined by Eq. (1), i.e. the newly inserted vertices are computed as a linear combination of old neighboring vertices. For clarity and easy implementation, Eq. (1) is often represented by a subdivision mask as shown in Fig. 3. A newly inserted vertex (black dot) is computed as a linear combination of the old vertices (in circle).

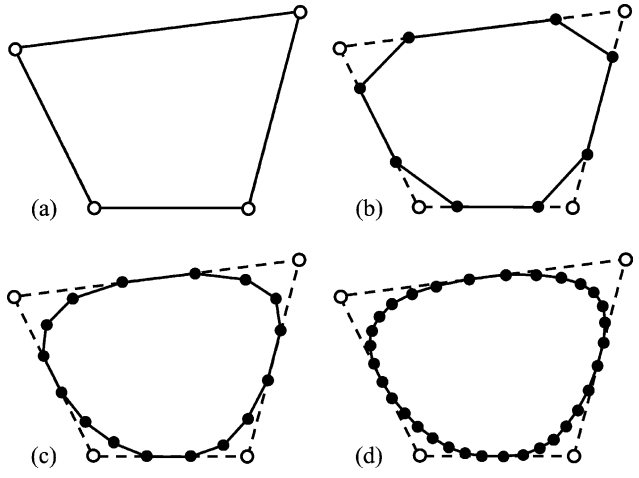

Fig. 1. Subdivision through Chaikin's corner cutting algorithm: (a) the initial control mesh; (b)–(d) control meshes after one, two and three subdivisions, respectively.

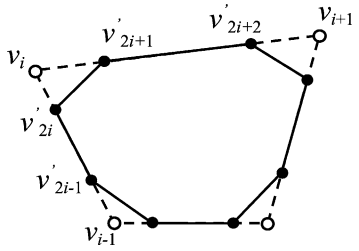

Fig. 2. Topological rules for Chinkin's subdivision.

The coefficients are marked above the corresponding vertices.

$$v'_{2i} = \tfrac{1}{4}v_{i-1} + \tfrac{3}{4}v_i \tag{1a}$$

$$v'_{2i+1} = \tfrac{3}{4}v_i + \tfrac{1}{4}v_{i+1} \tag{1b}$$

2.2. Doo–Sabin subdivision surfaces

A generalization of the tensor product version of Chaikin's subdivision is known as Doo–Sabin subdivision surfaces widely discussed in literature. For a regular rectangular control mesh, Doo–Sabin subdivision produces uniform bi-quadratic B-spline surfaces in the limit. For an arbitrary control mesh, it produces a global C1 continuous limit surface. Doo–Sabin subdivision surfaces are defined by the following set of topological and geometric rules.

- The topological rules of Doo–Sabin surfaces are shown in Fig. 4. For each face with n-vertices, n newly inserted vertices are computed following the geometric rules discussed in the next item. The new refined mesh is constructed by connecting related vertices to form F-, E- and V-faces as shown in Fig. 4. For each old face, a new F-face is constructed by connecting all newly inserted vertices of the corresponding face. For each old edge, a new E-face can also be constructed by connecting the four corresponding newly inserted vertices incident to that edge. For each old vertex, a V-face can also be constructed by connecting all corresponding newly inserted vertices incident to the old vertex.
- The geometric rule is again defined as a linear combination of all related old vertices. The subdivision masks of the geometric rules are shown in Fig. 5 and are defined by Eq. (2).

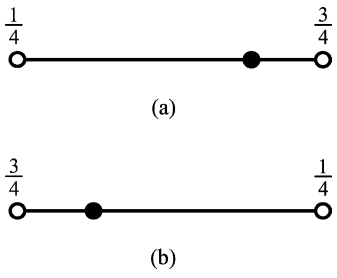

Fig. 3. Masks for Chinkin's subdivision.

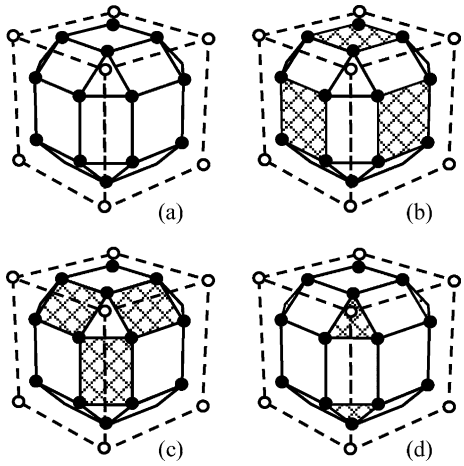

Fig. 4. Topological rules for Doo–Sabin subdivision: (a) general topological connection after mesh refinement; (b) *F*-face construction; (c) *E*-face construction; and (d) *V*-face construction.

For regular faces with four sides, the subdivision mask is shown in Fig. 5(a) and is defined by Eq. (2a).

$$v' = \tfrac{9}{16}v_0 + \tfrac{3}{16}v_1 + \tfrac{1}{16}v_2 + \tfrac{3}{16}v_3 \tag{2a}$$

For irregular faces, the mask is shown in Fig. 5(b) and newly inserted vertices are defined by Eq. (2b)

$$v' = \sum_{i=0}^{n-1} \alpha_i v_i \tag{2b}$$

Doo and Sabin [10] suggested to use the following coefficients

$$\alpha_i = \begin{cases} \dfrac{n+5}{4n} & \text{for } i = 0 \\ \dfrac{3 + 2\cos(2\pi i/n)}{4n} & \text{for } i = 1, 2, \ldots, n-1 \end{cases} \tag{3a}$$

Alternatively, one may also use the following formulas proposed by Catmull and Clark [6]

$$\alpha_i = \begin{cases} \dfrac{1}{2} + \dfrac{1}{4n} & \text{for } i = 0 \\ \dfrac{1}{8} + \dfrac{1}{4n} & \text{for } i = 1, n-1 \\ \dfrac{1}{4n} & \text{for } i = 2, \ldots, n-2 \end{cases} \tag{3b}$$

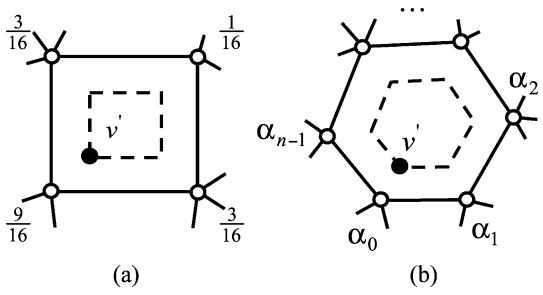

Fig. 5. Masks for Doo–Sabin subdivision: (a) for regular faces with four edges; and (b) for an irregular *n*-sided face.

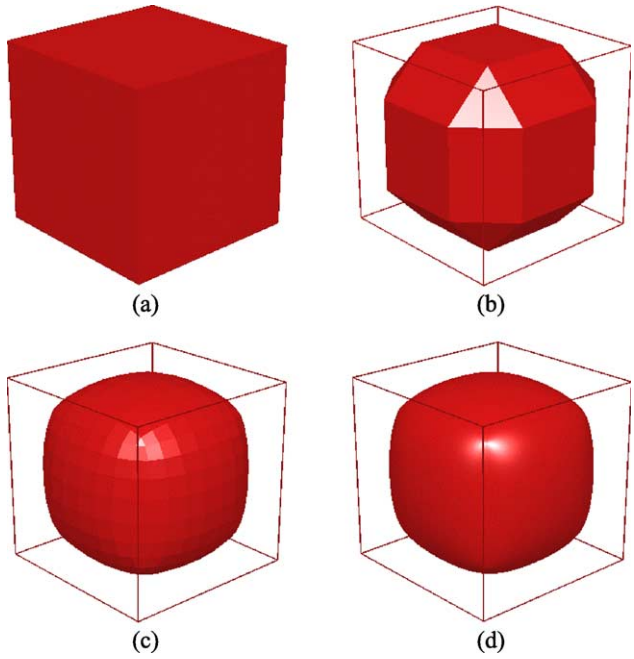

Fig. 6. Illustration of a Doo–Sabin subdivision surface [6,10]: (a) the initial control mesh; (b) the control mesh after one level of refinement; (c) the control mesh after three refinements; and (d) the limit surface.

Fig. 6 shows a Doo–Sabin surface defined by control vertices shown in Fig. 6(a). In this example, Eq. (3b) is used for computing newly inserted vertices on irregular faces. It should be noted that there is no need to do infinitive number of subdivisions for limit surface evaluation. As it will be discussed in Section 4, the limit surface mesh can be produced at any level of subdivision in a single step.

3. Subdivision schemes from B-splines

Doo–Sabin surfaces discussed in Section 2 are generalizations of uniform bi-quadratic B-spline surfaces. Catmull–Clark surfaces are, on the other hand, generalizations of uniform bi-cubic B-spline surfaces. In literature, many subdivision schemes are further generalizations of a subset of splines. In this section, we show how subdivision schemes, such as Doo–Sabin and Catmull–Clark surfaces, can be constructed from B-spline mathematics.

3.1. Refinement of B-splines

We first examine the refinement property of B-splines. For notational simplicity, we consider a set of uniform knots $\{t_i\}_{i=-\infty}^{+\infty} = \{i\}_{i=-\infty}^{+\infty}$. All basis functions of order k are actually translations of the same basis function $B_k(t)$. In addition, the basis function can also be defined as a linear combination of $k+1$ translated (with index j) and dilated (with new parametrization $2t$) copy of itself using the following refinement equation [61]

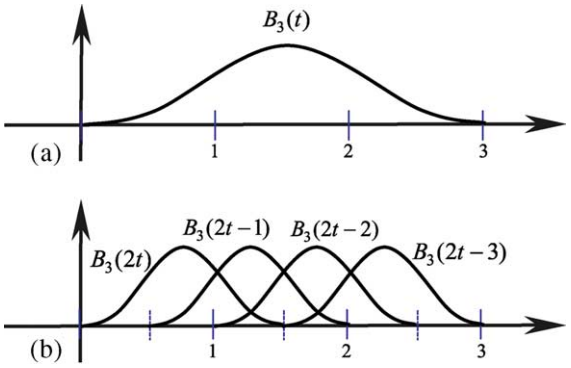

Fig. 7. Refinement of a third-order B-spline basis function through translation and dilation: (a) original basis function; and (b) translated and dilated copies of itself.

$$B_k(t) = \frac{1}{2^{k-1}} \sum_{j=0}^{k} \binom{k}{j} B_k(2t-j) \tag{4}$$

All subdivision schemes generalizing uniform B-splines can be derived based on Eq. (4).

3.2. Curve subdivision scheme construction

As an example, the Chaikin's subdivision can be derived from Eq. (4) with order 3. Fig. 7 shows this case and the refinement is defined as:

$$B_3(t) = \tfrac{1}{4}B_3(2t) + \tfrac{3}{4}B_3(2t-1) + \tfrac{3}{4}B_3(2t-2) + \tfrac{1}{4}B_3(2t-3) \tag{5}$$

For clarity, we illustrate all the basis functions of a uniform quadratic B-spline curve before and after mid point knot insertion in Fig. 8. Based on the refinement of Eq. (5) and noting the notational changes in writing the refined basis functions between Figs. 7 and 8, we have

$$\begin{aligned}
p(t) &= \sum_{i=-\infty}^{+\infty} v_i B_{i,3}(t) \\
&= \cdots + v_{i-1}\left(\frac{1}{4}B'_{2i-3,3}(t) + \frac{3}{4}B'_{2i-2,3}(t) + \frac{3}{4}B'_{2i-1,3}(t) + \frac{1}{4}B'_{2i,3}(t)\right) + v_i\left(\frac{1}{4}B'_{2i-1,3}(t) + \frac{3}{4}B'_{2i,3}(t) + \frac{3}{4}B'_{2i+1,3}(t) + \frac{1}{4}B'_{2i+2,3}(t)\right) + v_{i+1}\left(\frac{1}{4}B'_{2i+1,3}(t) + \frac{3}{4}B'_{2i+2,3}(t) + \frac{3}{4}B'_{2i+3,3}(t) + \frac{1}{4}B'_{2i+4,3}(t)\right) \\
&= \cdots + \left(\frac{3}{4}v_{i-1} + \frac{1}{4}v_i\right)B'_{2i-1,3}(t) + \left(\frac{1}{4}v_{i-1} + \frac{3}{4}v_i\right)B'_{2i,3}(t) \\
&\quad + \left(\frac{3}{4}v_i + \frac{1}{4}v_{i+1}\right)B'_{2i+1,3}(t) + \left(\frac{1}{4}v_i + \frac{3}{4}v_{i+1}\right)B'_{2i+2,3}(t) + \cdots \\
&= \cdots + v'_{2i-1}B'_{2i-1,3}(t) + v'_{2i}B'_{2i,3}(t) + v'_{2i+1}B'_{2i+1,3}(t) + v'_{2i+2}B'_{2i+2,3}(t) + \cdots = \sum_{i=-\infty}^{+\infty} v'_i B'_{i,3}(t)
\end{aligned} \tag{6}$$

where v'_{2i} and v'_{2i+1} represent vertices after refinement and are defined as the following linear combinations of the original vertices v_{i-1}, v_i and v_{i+1}

$$v'_{2i} = \tfrac{1}{4}v_{i-1} + \tfrac{3}{4}v_i \tag{7a}$$

$$v'_{2i+1} = \tfrac{3}{4}v_i + \tfrac{1}{4}v_{i+1} \tag{7b}$$

Eq. (7) is exactly the same as Eq. (1), i.e. the Chaikin's subdivision discussed in Section 2. The subdivision masks are shown in Figs. 2 and 3.

Following Eq. (4), we can also refine a fourth-order basis function as follows

$$B_4(t) = \tfrac{1}{8}B_4(2t) + \tfrac{1}{2}B_4(2t-1) + \tfrac{3}{4}B_4(2t-2) + \tfrac{1}{2}B_4(2t-3) + \tfrac{1}{8}B_4(2t-4) \tag{8}$$

Fig. 9 shows the refinement of uniform cubic B-spline basis functions with the same notations as that shown in Fig. 8 for quadratic B-spline curve refinement. Following Eq. (8), Fig. 9 and related notations, the refinement equation for a cubic B-spline curve can be refined as:

$$\begin{aligned}
p(t) &= \sum_{i=-\infty}^{+\infty} v_i B_{i,4}(t) \\
&= \cdots + v_{i-1}\left(\frac{1}{8}B'_{2i-4,4} + \frac{1}{2}B'_{2i-3,4} + \frac{3}{4}B'_{2i-2,4} + \frac{1}{2}B'_{2i-1,4} + \frac{1}{8}B'_{2i,4}\right) + v_i\left(\frac{1}{8}B'_{2i-2,4} + \frac{1}{2}B'_{2i-1,4} + \frac{3}{4}B'_{2i,4} + \frac{1}{2}B'_{2i+1,4} + \frac{1}{8}B'_{2i+2,4}\right) \\
&\quad + v_{i+1}\left(\frac{1}{8}B'_{2i,4} + \frac{1}{2}B'_{2i+1,4} + \frac{3}{4}B'_{2i+2,4} + \frac{1}{2}B'_{2i+3,4} + \frac{1}{8}B'_{2i+4,4}\right) \\
&= \cdots + \left(\frac{1}{8}v_{i-1} + \frac{3}{4}v_i + \frac{1}{8}v_{i+1}\right)B'_{2i,4}(t) + \left(\frac{1}{2}v_i + \frac{1}{2}v_{i+1}\right)B'_{2i+1,4}(t) + \cdots
\end{aligned}$$

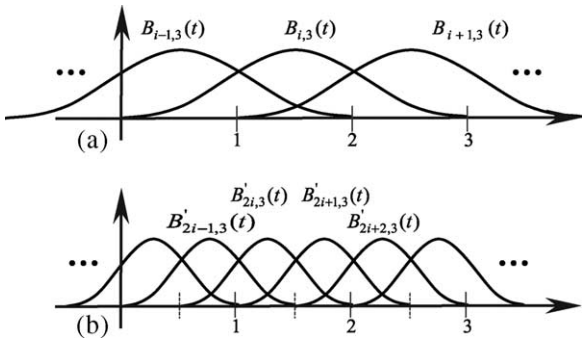

Fig. 8. Refinement of quadratic B-splines through mid-point knot insertion (binary refinement): (a) basis functions defined by a set of uniform knots; and (b) basis functions defined by refined knots through mid-point insertion.

$$= \cdots + v'_{2i}B'_{2i,4}(t) + v'_{2i+1}B'_{2i+1,4}(t) + \cdots$$
$$= \sum_{i=-\infty}^{+\infty} v'_i B'_{i,4}(t) \tag{9}$$

Based on the above derivation, we obtain the following equation for cubic B-spline curve subdivision

$$v'_{2i} = \tfrac{1}{8}v_{i-1} + \tfrac{3}{4}v_i + \tfrac{1}{8}v_{i+1} \tag{10a}$$

$$v'_{2i+1} = \tfrac{1}{2}v_i + \tfrac{1}{2}v_{i+1} \tag{10b}$$

Figs. 10 and 11 summarize the topological and geometric rules, respectively. For each refinement, each of the old vertices is updated and a new vertex is inserted for each edge. The subdivision masks are shown in Fig. 11.

3.3. Surface subdivision scheme construction

For B-spline surfaces, we can also construct various subdivision schemes based on tensor product formulation. We take the Catmull–Clark subdivision surface as an example and construct the scheme based on extensions of refinement of uniform bi-cubic B-spline surfaces. For

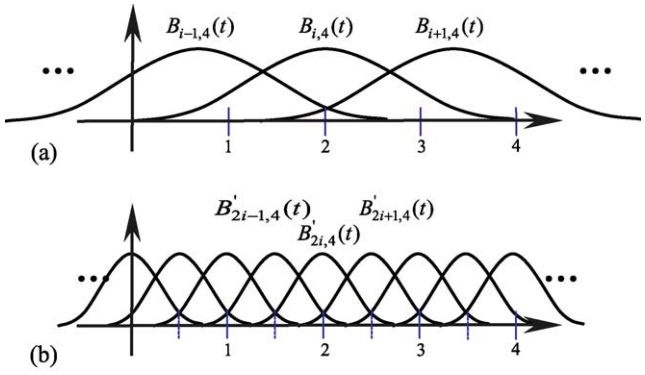

Fig. 9. Refinement of cubic B-splines through mid-point knot insertion (binary refinement): (a) basis functions defined by a set of uniform knots; and (b) basis functions defined by refined knots through mid-point insertion.

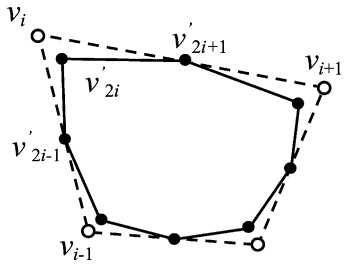

Fig. 10. Topological rules for cubic spline curve subdivision.

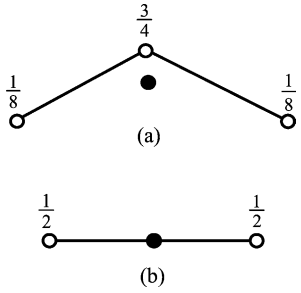

Fig. 11. Masks for cubic spline curve subdivision: (a) masks for updated corner vertices; and (b) mask for newly inserted edge vertex.

notational simplicity, we rewrite Eq. (8) as follows:

$$B_{i,k}(t) = \sum_{l=0}^{k} \alpha_l B_{i,k}(2t-l) = \sum_{l=0}^{k} \alpha_l B'_{2i-k+2+l}(t)$$
$$= \sum_{l=0}^{4} \alpha_l B'_{2i-2+l}(t) \tag{11}$$

with $k=4$ and $\{\alpha_l\}_{l=0}^{4} = \{\frac{1}{8}, \frac{1}{2}, \frac{3}{4}, \frac{1}{2}, \frac{1}{8}\}$. We have then the following refinement for bi-cubic tensor product B-spline surfaces

$$p(u,v) = \sum_{i=-\infty}^{+\infty}\sum_{j=-\infty}^{+\infty} v_{ij}B_i(u)B_j(v) = \sum_{i=-\infty}^{+\infty}\sum_{j=-\infty}^{+\infty} v_{ij}B_{ij}(u,v)$$
$$= \cdots + v_{i-1,j-1}\sum_{l=0}^{4}\alpha_l B'_{2(i-1)-2+l}\sum_{l=0}^{4}\alpha_l B'_{2(j-1)-2+l}$$
$$+ v_{i,j-1}\sum_{l=0}^{4}\alpha_l B'_{2i-2+l}\sum_{l=0}^{4}\alpha_l B'_{2(j-1)-2+l}$$
$$+ v_{i+1,j-1}\sum_{l=0}^{4}\alpha_l B'_{2(i+1)-2+l}\sum_{l=0}^{4}\alpha_l B'_{2(j-1)-2+l}$$
$$+ v_{i-1,j}\sum_{l=0}^{4}\alpha_l B'_{2(i-1)-2+l}\sum_{l=0}^{4}\alpha_l B'_{2j-2+l}$$
$$+ v_{i,j}\sum_{l=0}^{4}\alpha_l B'_{2i-2+l}\sum_{l=0}^{4}\alpha_l B'_{2j-2+l}$$
$$+ v_{i+1,j}\sum_{l=0}^{4}\alpha_l B'_{2(i+1)-2+l}\sum_{l=0}^{4}\alpha_l B'_{2j-2+l}$$
$$+ v_{i-1,j+1}\sum_{l=0}^{4}\alpha_l B'_{2(i-1)-2+l}\sum_{l=0}^{4}\alpha_l B'_{2(j+1)-2+l}$$

$$+ v_{i,j+1} \sum_{l=0}^{4} \alpha_l B'_{2i-2+l} \sum_{l=0}^{4} \alpha_l B'_{2(j+1)-2+l}$$
$$+ v_{i+1,j+1} \sum_{l=0}^{4} \alpha_l B'_{2(i+1)-2+l} \sum_{l=0}^{4} \alpha_l B'_{2(j+1)-2+l+\ldots} \quad (12)$$

After expanding the terms and reorganization following the refined basis functions, we obtain

$$p(u,v) = \sum_{i=-\infty}^{+\infty} \sum_{j=-\infty}^{+\infty} v_{ij} B_{ij}(u,v) = \cdots + v'_{2i,2j} B'_{2i,2j}(u,v) + v'_{2i+1,2j} B'_{2i+1,2j}(u,v) + v'_{2i,2j+1} B'_{2i,2j+1}(u,v) + v'_{2i+1,2j+1} B'_{2i+1,2j+1}(u,v) + \cdots \quad (13)$$

where

$$\begin{aligned} v'_{2i,2j} &= \tfrac{1}{64}(v_{i-1,j-1} + 6v_{i,j-1} + v_{i+1,j-1} + 6v_{i-1,j} + 36v_{i,j} + 6v_{i+1,j} + v_{i-1,j+1} + 6v_{i,j+1} + v_{i+1,j+1}) \\ v'_{2i+1,2j} &= \tfrac{1}{16}(v_{i,j-1} + v_{i+1,j-1} + 6v_{i,j} + 6v_{i+1,j} + v_{i,j+1} + v_{i+1,j+1}) \\ v'_{2i,2j+1} &= \tfrac{1}{16}(v_{i-1,j} + v_{i-1,j+1} + 6v_{i,j} + 6v_{i,j+1} + v_{i+1,j} + v_{i+1,j+1}) \\ v'_{2i+1,2j+1} &= \tfrac{1}{4}(v_{i,j} + v_{i+1,j} + v_{i,j+1} + v_{i+1,j+1}) \end{aligned} \quad (14)$$

are the refined control vertices that are defined as a linear combination of neighboring old vertices. Following Eq. (14), the refined control vertices can be classified into three classes as shown in Fig. 12, i.e. newly inserted face vertices (*F*-vertices) $F'_{2i+1,2j+1} = v'_{2i+1,2j+1}$, updated vertex vertices (*V*-vertices) $V_{2i,2j} = v'_{2i,2j}$, and two newly inserted edge vertices (*E*-vertices) $E_{2i+1,2j} = v'_{2i+1,2j}$ and $E_{2i,2j+1} = v'_{2i,2j+1}$. Fig. 13(a), (c) and (d) shows the masks for uniform bi-cubic B-spline surface subdivision.

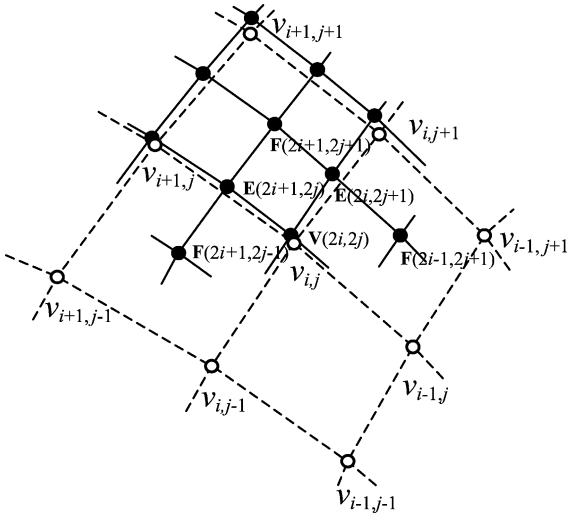

Fig. 12. Subdivision of uniform bi-cubic B-spline surfaces. In this figure, circle vertices are old vertices before refinement, black vertices are newly updated/inserted vertices after refinement, vertices such as $F(2i+1,2j+1)$ are newly inserted face vertices (*F*-vertices), vertices such as $V(2i,2j)$ are newly updated vertex vertices (*V*-vertices) of $v'_{2i,2j}$, and vertices such as $E(2i+17,2j)$ or $E(2i,2j+1)$ are newly inserted edge vertices (*E*-vertices).

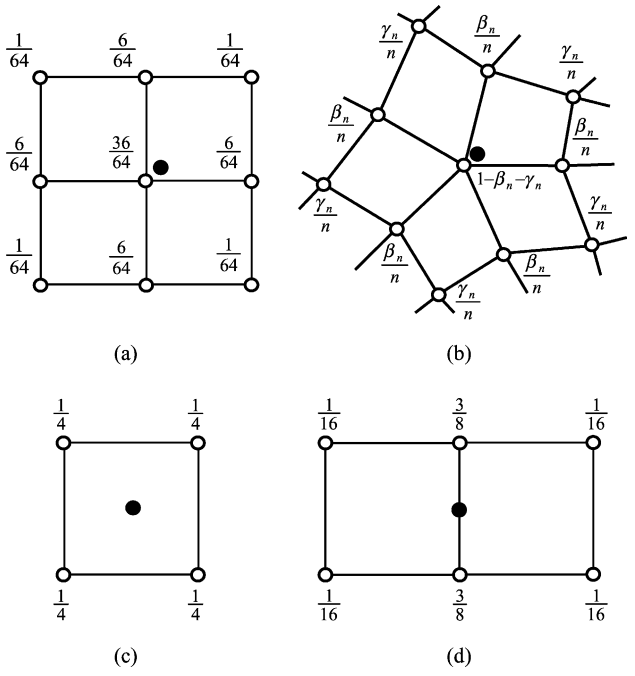

Fig. 13. Catmull–Clark subdivision masks for quadrilateral meshes: (a) updated regular *V*-vertices; (b) updated general *V*-vertices; (c) newly inserted F-vertices; and (d) newly inserted *E*-vertices. In this figure, $\beta_n = 3/2n$ and $\gamma_n = 1/4n$.

To extend the subdivision to general quadrilateral mesh of arbitrary topology, the refinement of $v'_{2i,2j}$ in Eq. (14) can be rewritten as

$$v'_{2i,2j} = \left(1 - \frac{3}{8} - \frac{1}{16}\right) v_{i,j} + \frac{3/8}{4}(v_{i,j-1} + v_{i-1,j} + v_{i+1,j} + v_{i,j+1}) + \frac{1/16}{4}(v_{i-1,j-1} + v_{i+1,j-1} + v_{i-1,j+1} + v_{i+1,j+1}) \quad (15)$$

Now let n be the number of edges incident to vertex v_i, called valence of the corresponding vertex ($n=4$ for regular vertices), $\beta_n = 3/2n$ and $\gamma_n = 1/4n$ be two coefficients for updating the *V*-vertices ($\beta_4 = 3/8$ and $\gamma_4 = 1/16$ for regular vertices),

$$\{p_k\}_{k=0}^{n-1} = \{v_{i,j-1}, v_{i-1,j}, v_{i+1,j}, v_{i,j+1}\}$$

be a collection of edge vertices incident to v_{ij}, and

$$\{q_k\}_{k=0}^{n-1} = \{v_{i-1,j-1}, v_{i+1,j-1}, v_{i-1,j+1}, v_{i+1,j+1}\}$$

be a collection of the opposite corner vertices of v_{ij} of faces incident to v_{ij}. The refined control vertices of Eq. (14) can then written as

$$\begin{aligned}
v'_{2i,2j} &= (1-\beta_n-\gamma_n)v_{i,j} + \frac{\beta_n}{n}\sum_{i=0}^{n-1} p_i + \frac{\gamma_n}{n}\sum_{i=0}^{n-1} q_i \\
v'_{2i+1,2j} &= \frac{1}{16}(v_{i,j-1} + v_{i+1,j-1} + 6v_{i,j} + 6v_{i+1,j} \\
&\quad + v_{i,j+1} + v_{i+1,j+1}) \\
v'_{2i,2j+1} &= \frac{1}{16}(v_{i-1,j} + v_{i-1,j+1} + 6v_{i,j} + 6v_{i,j+1} \\
&\quad + v_{i+1,j} + v_{i+1,j+1}) \\
v'_{2i+1,2j+1} &= \frac{1}{4}(v_{i,j} + v_{i,j+1} + v_{i+1,j} + v_{i+1,j+1})
\end{aligned} \tag{16a}$$

with the following coefficients

$$\beta_n = \frac{3}{2n} \text{ and } \gamma_n = \frac{1}{4n} \tag{16b}$$

Eq. (16) can thus be used for general quadrilateral meshes of arbitrary topology and it reduces to Eq. (14) for regular vertices with valence $n=4$. This leads to the well-known Catmull–Clark subdivision for quadrilateral meshes of arbitrary topology. Fig. 13 shows all related subdivision masks.

Eq. (16) can be further extended to a more general form for arbitrary control meshes (not just with quadrilateral faces). For this purpose, the newly inserted *V*-vertex $v'_{2i,2j}$ and *E*-vertices $v'_{2i+1,2j}$ and $v'_{2i,2j+1}$ of Eq. (14) can be reorganized based on the newly computed face vertices

$$\begin{aligned}
v'_{2i,2j} &= (1-\beta-\gamma)v_{i,j} + \frac{\beta}{n}(v_{i,j-1} + v_{i-1,j} + v_{i+1,j} + v_{i,j+1}) \\
&\quad + \frac{\gamma}{n}(v'_{2i-1,2j-1} + v'_{2i-1,2j+1} + v'_{2i+1,2j-1} + v'_{2i+1,2j+1}) \\
v'_{2i+1,2j} &= \frac{1}{4}(v_{i,j} + v_{i+1,j} + v'_{2i+1,2j-1} + v'_{2i+1,2j+1}) \\
v'_{2i,2j+1} &= \frac{1}{4}(v_{i,j} + v_{i,j+1} + v'_{2i-1,2j+1} + v'_{2i+1,2j+1})
\end{aligned} \tag{17a}$$

with the following coefficients

$$\beta = \gamma = 1/n, \tag{17b}$$

where, n again stands for the valence of the control mesh at vertex v_{ij}, and

$$\begin{aligned}
v'_{2i-1,2j-1} &= \frac{1}{n_f}(v_{i-1,j-1} + v_{i-1,j} + v_{i,j-1} + v_{i,j}) \\
v'_{2i-1,2j+1} &= \frac{1}{n_f}(v_{i-1,j} + v_{i-1,j+1} + v_{i,j} + v_{i,j+1}) \\
v'_{2i+1,2j-1} &= \frac{1}{n_f}(v_{i,j-1} + v_{i,j} + v_{i+1,j-1} + v_{i+1,j}) \\
v'_{2i+1,2j+1} &= \frac{1}{n_f}(v_{i,j} + v_{i,j+1} + v_{i+1,j} + v_{i+1,j+1})
\end{aligned} \tag{17c}$$

are the updated face vertices with $n_f=4$ being the number of vertices of the corresponding face. Please note that we omitted the subscript of β and γ in order not to be confused with Eq. (16), but both the two coefficients vary depending on the valance n. Now further let

$$\{p_k\}_{k=0}^{n-1} = \{v_{i,j-1}, v_{i-1,j}, v_{i+1,j}, v_{i,j+1}\}$$

be a collection of edge vertices incident to v_{ij} and let

$$\begin{aligned}
\{q_k\}_{k=0}^{n-1} &= \{v'_{2i-1,2j-1}, v'_{2i-1,2j+1}, v'_{2i+1,2j-1}, v'_{2i+1,2j+1}\} \\
&= \{F_{2i-1,2j-1}, F_{2i-1,2j+1}, F_{2i+1,2j-1}, F_{2i+1,2j+1}\}
\end{aligned}$$

be a collection of newly inserted face vertices (*F*-vertices) incident to vertex v_{ij}. The refined control vertices of Eq. (13) can then be represented in yet another form in terms of newly computed face vertices as:

$$\begin{aligned}
v'_{2i,2j} &= (1-\beta-\gamma)v_{i,j} + \frac{\beta}{n}\sum_{i=0}^{n-1} p_i + \frac{\gamma}{n}\sum_{i=0}^{n-1} q_i \\
v'_{2i,2j+1} &= \frac{1}{4}(v_{i,j} + v_{i,j+1} + F_{2i-1,2j+1} + F_{2i+1,2j+1}) \\
v'_{2i+1,2j} &= \frac{1}{4}(v_{i,j} + v_{i+1,j} + F_{2i+1,2j-1} + F_{2i+1,2j+1}) \\
v'_{2i+1,2j+1} &= \frac{1}{n_f}(v_{i,j} + v_{i,j+1} + v_{i+1,j} + v_{i+1,j+1})
\end{aligned} \tag{18a}$$

with coefficients as follows

$$\beta = \gamma = 1/n, \tag{18b}$$

Eq. (18) can now be easily extended to handle arbitrary control meshes. One can compute newly inserted F-vertices as an average of all old vertices of the corresponding face for arbitrary n_f and then use Eq. (18) with a general valence n. This leads to the Catmull–Clark subdivision in a more general form and can be summarized as follows:

- *F*-vertices: A face vertex for each face is computed as an average of all old control vertices of the corresponding face.
- *E*-vertices: An edge vertex for each edge is computed as an average of the two end vertices of the corresponding edge and the two newly inserted *F*-vertices whose faces share the same corresponding edge, i.e. an average of four related vertices.
- *V*-vertices: A vertex vertex is computed as a linear combination of the corresponding old vertex, all old

vertices incident to the corresponding vertex though edges, and all newly inserted face vertices whose faces incident to the corresponding vertex.

The refined V-vertices defined in Eq. (18a) are also often written in the following explicit form in terms of the valence n of v_{ij}.

$$v'_{2i,2j} = \frac{n-2}{n} v_{i,j} + \frac{1}{n^2} \sum_{i=0}^{n-1} p_i + \frac{1}{n^2} \sum_{i=0}^{n-1} q_i \tag{19}$$

In addition, subdivision rules for sharp feature, such as crease edges, boundary edges, corners where three or more creases meet, and darts where a crease edge terminates, can also be defined. We may keep all corners unchanged during the refinement (mask not shown in Fig. 15), use the subdivision rules for cubic curves defined by Eq.(10) and Figs. 10 and 11 for refining crease and boundary edges, and use the same mask as that for smooth vertices for dart vertices. Fig. 14 shows how exactly the refined control mesh is constructed. Fig. 15 shows the masks for Catmull–Clark subdivision in case of a general control mesh.

In case of extraordinary vertices whose valence is other than 4, i.e. $n \neq 4$, the coefficients β and γ in Eq. (18) can be selected from a wide range and can be optimized to achieve well behaved shape at the extraordinary corner positions. However, it should not be confused with Eq. (16) in computing V-vertices. Fig. 16 shows an example of a smooth Catmull–Clark subdivision surface model.

In a similar way, one may also develop a tensor product version subdivision scheme for quadratic B-spline surfaces based on the Chaikin's algorithm and extend it to well-known Doo–Sabin subdivision surfaces. In literature, one may find several other approaches in constructing various subdivision schemes and in optimizing existing subdivision schemes for better surface behaviour. In connection with schemes generalizing B-splines, further readings can be found in [42,43,47,50,62, and references therein].

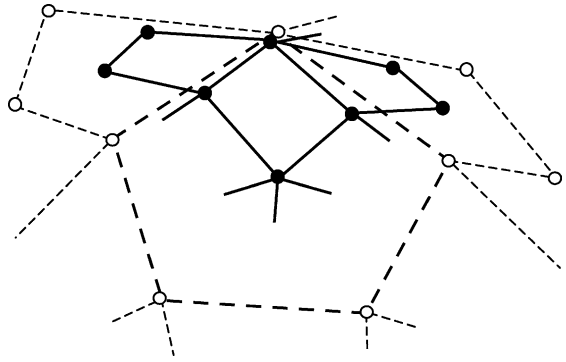

Fig. 14. Topological rules for Catmull–Clark subdivision surfaces.

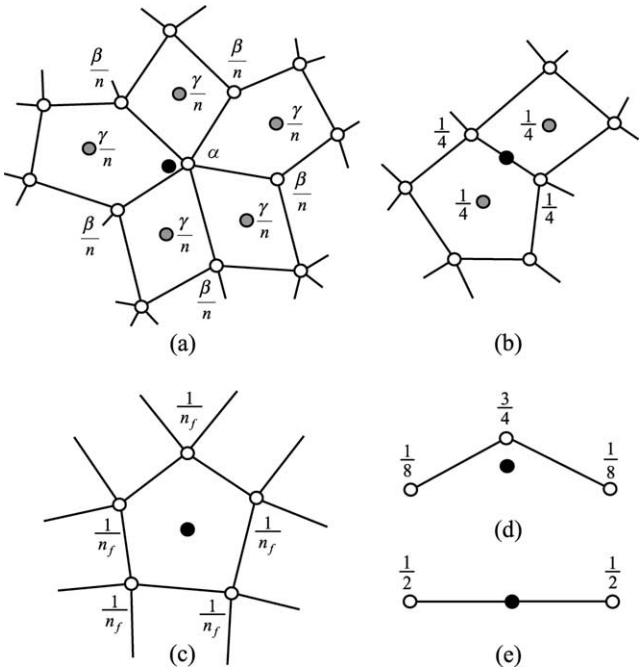

Fig. 15. General subdivision masks for Catmull–Clark surfaces: (a) mask for updated smooth V-vertices and darts; (b) mask for newly inserted E-vertices; and (c) mask for newly inserted face vertices; (d) mark for updated crease/boundary V-vertices; and (e) mark for newly inserted crease/boundary E-verices. In this figure, $\beta=\gamma=1/n$ and $\alpha=1-\beta-\gamma$ (or $\alpha+\beta+\gamma=1$), and vertices with gray shading are newly inserted face vertices.

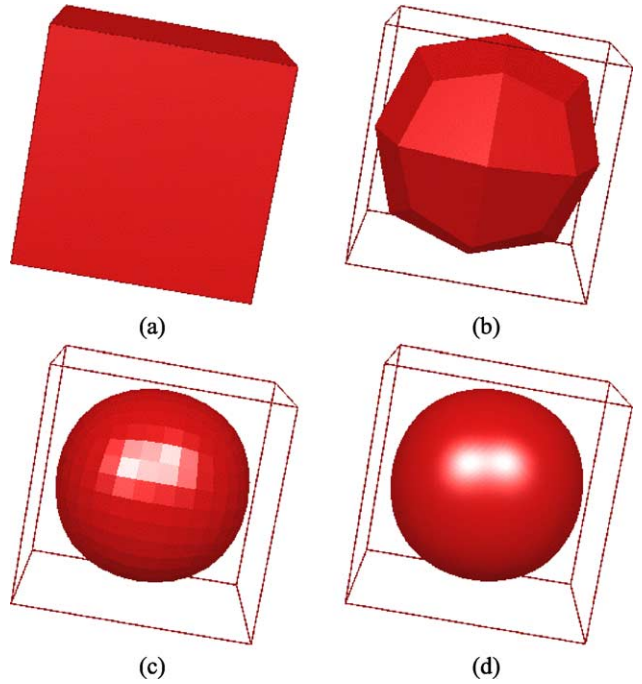

Fig. 16. Illustration of a Catmull–Clark subdivision surface [6]: (a) the initial control mesh; (b) the control mesh after one level of refinement; (c) the control mesh after three refinement; and (d) the limit surface.

4. Overview of subdivision schemes

In literature, one may find rich families of subdivision schemes. While most of the reported schemes are further generalizations of a subset of splines [6,10,39,50,62], some other subdivision schemes are further extensions of box-splines [22,27,50]. There are also some subdivision schemes that are discrete versions of other functions, their analytic version do not exists or are not known at the moment [11,19,35].

4.1. Key concepts and a brief overview

As discussed in the Section 3, a subdivision scheme is defined by a set of topological rules and geometric rules for mesh refinement. Topological rules define how a control mesh is split into a refined mesh. Depending on the type of a subdivision scheme, typical operations of topological rules include insertion of new vertices into edges or faces, updating of old vertices, connection of newly inserted and updated vertices (with also old ones if applicable), and removal of some vertices, edges or faces. Geometric rules are used to compute the exact coordinates of the refined control vertices. When designing geometric rules for mesh subdivision, key properties need to be considered include affine invariance, finite support with small subdivision masks, symmetry, and behaviour of the limit surface. Techniques for series analysis, such as eigen structure analysis, z-transformtion and Fourier transformation, are often used to guide the selection of appropriate subdivision masks. Fig. 17 summarizes some basic topological rules for subdividing triangle and quadrilateral meshes. In literature, one may also find combined schemes that incorporate one or more of the topological rules summarized in Fig. 17 [35,51, 62]. Fig. 18 shows a Loop subdivision surface that use the one-to-four splitting topological rule for triangle meshes. Loop subdivision surfaces are generalizations of three-directional box-splines and further details about the scheme can be found in Refs. [16,27]. Fig. 19 shows a pipe model and a gun model produced using Doo–Sabin and Catmull–Clark subdivision surfaces, respectively.

In addition, the following is a list of important concepts in subdivision surface modeling:

- *Approximatory versus interpolatory*: If the limit surface of a subdivision scheme does not go through the initial

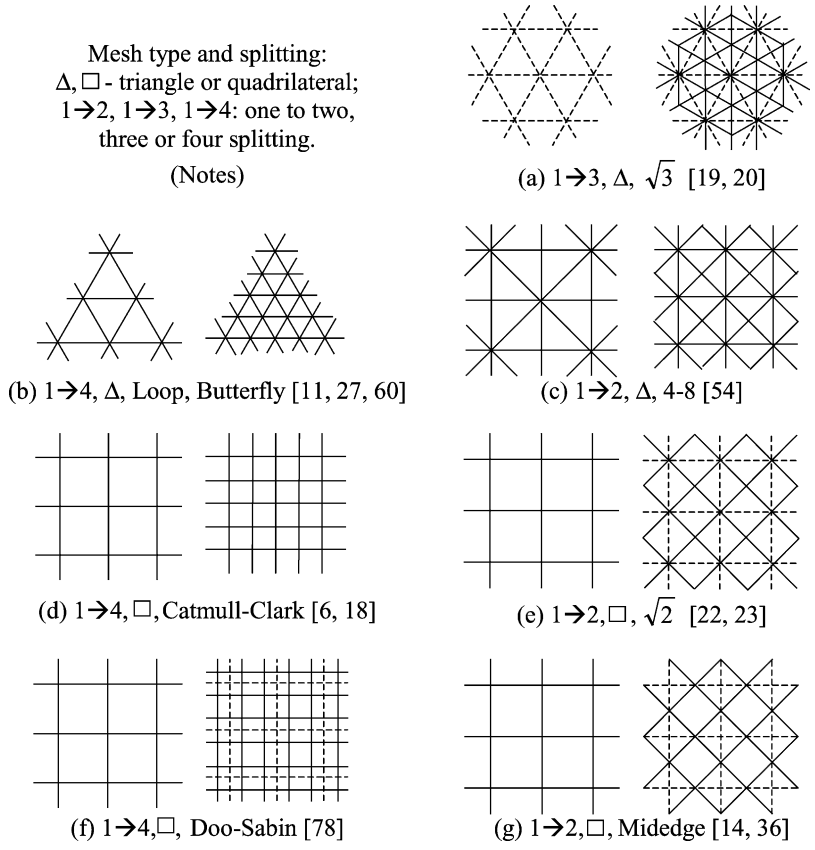

Fig. 17. Several important topological subdivision rules (illustrations showing meshes before and after subdivision): (a) $1\rightarrow3$ splitting for Δ meshes ($\sqrt{3}$ subdivision and interpolatory $\sqrt{3}$ subdivision [19,20]); (b) $1\rightarrow4$ splitting for Δ meshes (Loop and Butterfly subdivision [11,27,60]); (c) $1\rightarrow2$ splitting for paired Δ meshes (4–8 subdivision [54]); (d) $1\rightarrow4$ splitting for $\square$ meshes (Catmull–Clark subdivision [6,18]); (e) $1\rightarrow2$ splitting for $\square$ meshes ($\sqrt{2}$ subdivision and interpolatory $\sqrt{2}$ subdivision [22,23]); (f) $1\rightarrow4$ splitting for $\square$ meshes (Doo–Sabin subdivision [10]); (g) $1\rightarrow2$ splitting for $\square$ meshes (Midedge subdivision [14,36]).

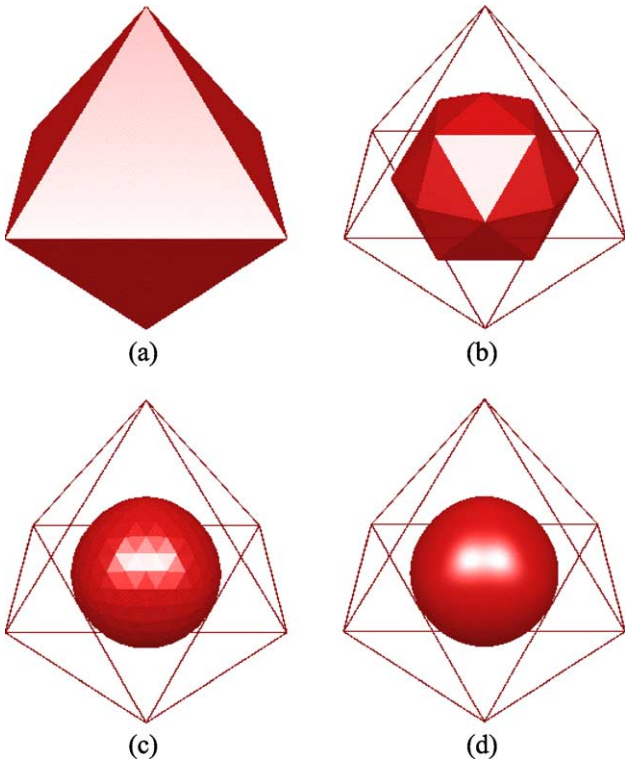

Fig. 18. Illustration of a Loop subdivision surface [27,46]: (a) the initial control mesh; (b) the control mesh after one level of refinement; (c) the control mesh after three refinement; and (d) the limit surface.

control points, the subdivision scheme is called an approximatory subdivision scheme. Examples of approximatory subdivision schemes include Loop subdivision [27], Doo–Sabin [10] and Catmull–Clark [6] subdivision surfaces. Otherwise, the scheme is an interpolatory subdivision scheme. Typical examples include an interpolatory Butterfly subdivision [11], Kobbelt subdivision [18], and an interpolatory $\sqrt{2}$ subdivision [23] and interpolatory $\sqrt{3}$ subdivision [20].

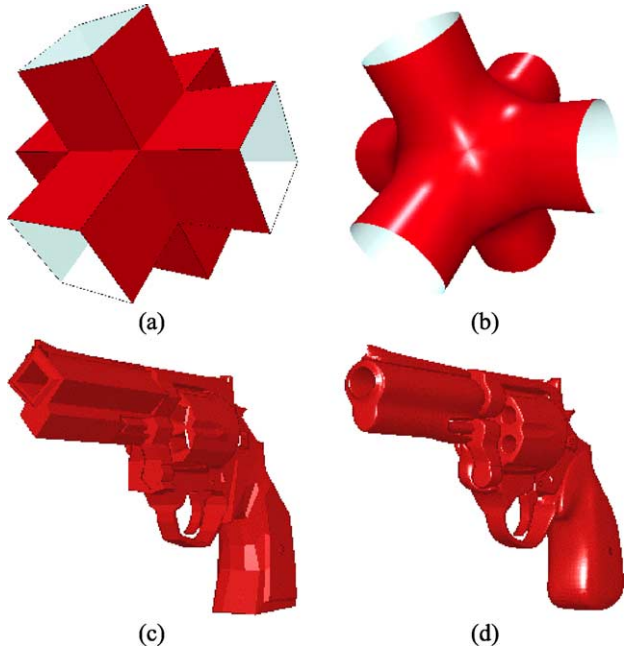

Fig. 19. Illustration of a pipe model (a) and (b) and a gun model (c) and (d) defined as a Doo–Sabin and Catmull–Clark surface, respectively. (a) and (c) initial control mesh, and (b) and (d) final limit surfaces.

- *Stationary versus non-stationary subdivision*: If the subdivision rules do not change during the subdivision process, the scheme is called a stationary subdivision scheme and, otherwise, a non-stationary subdivision scheme. Most of the existing subdivision schemes are stationary subdivision schemes. To produce certain classes of shapes, such as a perfect circle, a non-stationary subdivision scheme may have to be used [17,31].
- *Uniform versus non-uniform subdivision*: Most of the existing subdivision schemes are uniform subdivision schemes by which an existing mesh is refined uniformly through mid-point knot insertion over the entire surface for all levels of subdivision. Otherwise, it is called a non-uniform subdivision scheme. Most of the existing subdivision schemes are uniform subdivision schemes. The NURSS subdivision scheme [47] can, however, perform parametrized and non-uniform subdivision.
- *Global versus local or adaptive subdivision*: Most of the existing subdivision schemes are only designed to perform global subdivision. In certain situations, a local and adaptive subdivision might be desirable [32,48]. However, there are no existing subdivision schemes that can do adaptive subdivision without affecting the limit surface.

Many of the existing subdivision schemes can handle sharp features, such as crease and boundary edges [5,14,46,47]. Sharp features can be classified according to the number of vertices meeting at a vertex and the type of a vertex or an edge.

- *Edge classification*: We may distinguish three types of patch boundaries, i.e. an internal smooth edge where the limit surface is at least C1, a crease edge where the limit surface is C0, and a boundary edge where the surface terminates.
- *Vertex classification*: Let s be the number of crease edges meeting at a vertex. One can classify vertices into the following types according to the number of meeting crease edges s of the corresponding vertex.
  - A smooth vertex where the limit surface is at least C1 has no meeting crease edge with $s=0$.
  - A sharp vertex has no meeting crease edge with $s=0$, but the limit surface is not smooth at the vertex position. If the directional tangent of the limit surface at the vertex position does not vanish, the vertex is classified as a cone-type vertex. Otherwise, if the directional tangents of the limit surface at the vertex position vanish to a single vector, it is classified as a cusp vertex.

- A dart vertex is one where a crease edge terminates with $s=1$.
- A crease or boundary vertex is located on a crease or boundary edge, respectively, with $s=2$. A boundary vertex may also be defined as a corner vertex if the boundary curve is C0 and the surface goes through that vertex.
- A corner vertex has $s\geq 3$.

When handling sharp features, such as those for Catmull–Clark surfaces defined by the masks of Fig. 15(d) and (e), special rules need to be defined. Fig. 20 highlights some of the above mentioned crease features. In literature, one may find rich classes of subdivision rules for defining crease features for schemes, such as Loop, Doo–Sabin, Catmull–Clark subdivision schemes and NURSS [5,9,16, 34,46,47]. Most of the other schemes also have various ready definitions for commonly used crease features.

4.2. Properties of subdivision schemes

The analysis of subdivision surfaces at extraordinary corner or patch positions differ from that for regular parts of the control mesh. The later can often be deduced from the theory of the counter part of the scheme in continuous space, if available. For Catmull–Clark surfaces, e.g. the properties and continuity conditions of the limit surface on domains of regular grid of control points can be deduced from cubic B-spline surfaces, which is C2 continuous. Otherwise, limit surface properties can be analyzed using the same techniques as that for the analysis at extraordinary corner positions [2,8,12]. At extraordinary corner positions, properties of the limit surface can be studied using various tools for series analysis, such as z-transformation, Fourier transformation, and direct eigen structure analysis of the subdivision matrix of a small invariant stencil, i.e. a subset of the control mesh, of the corresponding subdivision scheme. The analysis of subdivision schemes near extraordinary corner positions was first addressed by Doo and Sabin in Ref. [10]. The properties were then studied by Ball and Storry in Refs. [1,2] and by Sabin in [41]. Further investigations were also carried out by Reif in Ref. [40] and Peters and Reif in Ref. [37]. One may also find some recent studies, such as [8,38,53,58,59]. At the moment, an elegant theoretical foundation has been established for the analysis of various properties, such as continuity conditions and surface interrogations of subdivision surfaces.

We again use Catmull–Clark surface to illustrate how the subdivision matrix can be set up and used for limit surface analysis, but the approach is the same for all stationary subdivision schemes. Fig. 21(a) shows the smallest invariant stencil (before and after subdivision) for

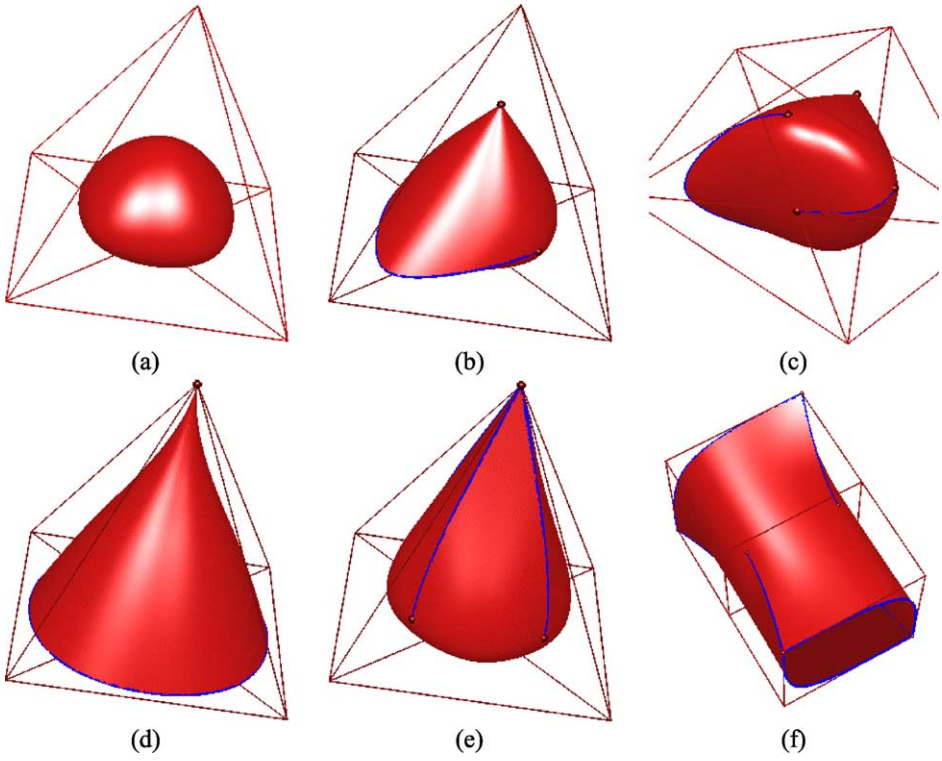

Fig. 20. Illustration of sharp features: (a) a smooth model without any sharp features; (b) and (c) a model with two crease edges, four darts and one conical tip in two different views; (d) a model with a closed crease edge and one cusp; (e) a model with four crease edges, four darts and one corner; (f) an open surface with two closed boundary edges, four internal crease edges, four darts and four external corners. In these illustrations, (a)–(e) are produced with the same control mesh, but marked with different sharp features. Illustrations (a)–(c) are produced with Loop subdivision surfaces and (d)–(f) are produced with Catmull–Clark surfaces.

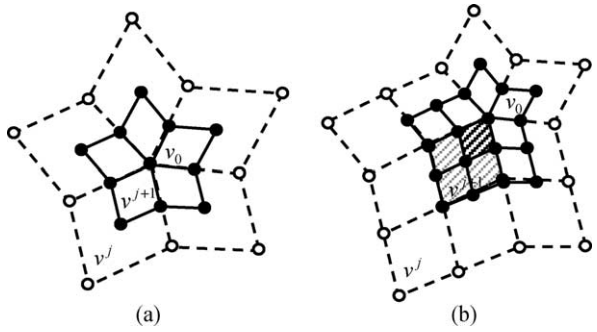

Fig. 21. Important invariant stencils of Catmull–Clark surfaces [15,49,61]: (a) stencil with $m = 2n + 1$ vertices for query and interrogation (one ring for evaluation) or $m = 6n + 1$ vertices for surface property analysis (two rings for continuity and curvature analysis) at extraordinary corner position v_0; and (b) stencil with $K=2n+8$ vertices for defining an extraordinary corner surface patch. In this figure, the valence of the extraordinary corner is $n=5$.

Catmull–Clark surface property evaluation or analysis at extraordinary corner position v_0. In the limit, this stencil converges to a point on the limit surface corresponding to v_0. Fig. 21(b) shows another invariant stencil (before and after subdivision) for defining an extraordinary corner patch of Catmull–Clark surfaces at v_0. This stencil is used in Section 4.3 in setting up another subdivision matrix for parametric evaluation of extraordinary corner patches of Catmull–Clark surfaces.

For surface property evaluation or analysis at vertex/corner positions, the stencil of Fig. 21(a) is used. Let $v^j = [v_0^j, v_1^j, \ldots, v_{m-1}^j]^T$ and $v^{j+1} = [v_0^{j+1}, v_1^{j+1}, \ldots, v_{m-1}^{j+1}]^T$ be a collection of the control points of the stencil before and after subdivision, respectively. The subdivision equation can be defined as

$$\begin{bmatrix} v_0^{j+1} \\ v_1^{j+1} \\ \vdots \\ v_{m-1}^{j+1} \end{bmatrix} = S \begin{bmatrix} v_0^{j} \\ v_1^{j} \\ \vdots \\ v_{m-1}^{j} \end{bmatrix} \tag{20}$$

or $v^{j+1} = Sv^j$ in short, with S being the subdivision matrix. Various properties of the limit surface at v_0 can be determined through direct eigen structure analysis of the subdivision matrix S. The eigen analysis of the subdivision matrix, in turn, is also critical for designing well behaved subdivision masks, i.e. to carefully select subdivision masks and coefficients that lead to desired eigen structures and consequently well-behaved surface properties.

Let us now assume that the subdivision matrix S has eigen values $\{\lambda_0,\lambda_1,\ldots,\lambda_{m-1}\}$ and corresponding left eigen vectors $\{x_0,x_1,\ldots x_{m-1}\}$, respectively, with eigen values organized in decreasing moduli $|\lambda_i| \geq |\lambda_{i+1}|$. The following summarizes some important properties of subdivision surfaces in relation to the eigen structure of the subdivision matrix [15,40,46,51,58,59]:

- *Affine invariance*: The subdivision scheme is affine invariant if and only if

$$\lambda_0 = 1. \tag{21}$$

- *Convergence*: A subdivision scheme converges if and only if $1=\lambda_0>\lambda_1$. Otherwise, the subdivision scheme would diverge if $\lambda_0>1$ and the control point/mesh would shrink to the origin if $\lambda_0<1$.
- *C1 continuity*: The corresponding limit position of the control vertex v_0 is C1 continuous provided that (a) the characteristic map of the subdivision is regular and injective, and (b) the sub-dominant eigenvalues satisfy

$$1 = \lambda_0 > \lambda_1 \geqslant \lambda_2 > \lambda_3 \cdots \tag{22a}$$

or preferably the following for binary subdivision schemes

$$1 = \lambda_0 > \frac{1}{2} = \lambda_1 = \lambda_2 > \lambda_3 \cdots. \tag{22b}$$

- *Bounded curvature*: The quality of curvature can be evaluated by

$$\rho = \lambda_3/\lambda_1^2. \tag{23}$$

In case $\rho<1$, one obtains flat/zero curvature. In case $\rho>1$, the curvature would diverge. Only in case $\rho=1$, one achieves bounded curvature. For well behaved binary subdivision surfaces, e.g., the sub-dominant eigenvalue should satisfy

$$1 = \lambda_0 > \frac{1}{2} = \lambda_1 = \lambda_2 > \frac{1}{4} = \lambda_3 = \lambda_4 = \lambda_5 > \lambda_6 \cdots \tag{24}$$

for obtaining bounded curvature at the limit position.
- *Query and interrogation*: The corresponding limit position of a control vertex v_0 is defined by

$$v_0^{\infty} = x_0^T v^0. \tag{25}$$

The tangent vectors at the limit position are defined by

$$c_1 = x_1^T v^0 \text{ and } c_2 = x_2^T v^0. \tag{26}$$

The surface normal is defined by

$$n = c_1 \times c_2. \tag{27}$$

The characteristic map of an n-valence vertex is defined as the planar limit surface whose initial control net is defined by the two right eigenvectors corresponding to the two subdominat eigenvalues λ_1 and λ_2, respectively [40,46,59]. For constructing the characterstic map, one may use a larger stencil for setting up the subdivision matrix, usually with one more ring control points than the smallest invariant stencil for analysis. Note that most of the subdivision schemes, such as the original Catmull–Clark surfaces discussed in Section 3, only achieve C1 continuity at extraordinary corner positions.

4.3. Parametric evaluation

Following the discussions of Section 4.2, it is possible to evaluate the corresponding limit position, the tangent vectors and surface normal of a control vertex at any resolution in a single step. In addition, there also exists an explicit analytical form for parametric evaluation of subdivision surfaces at an arbitrary position without going through the process of infinitive subdivision. Following the derivation reported in Ref. [49] for Catmull–Clark surfaces, such a parametric evaluation exists for all stationary subdivision schemes whose regular parts are extensions of a known form in the continuous domain, which is true for most of the existing subdivision schemes found in literature. Although it has not be reported till the moment, some kind of parametric evaluation might also exist for other stationary and non-stationary subdivision schemes and might be derived based on the analysis of the subdivision scheme through various approaches for analyzing the subdivision series.

Let us take the Catmull–Clark surface [49] as an example. For regular patches, the surface can be evaluated based on uniform bi-cubic B-spline surfaces as follows:

$$p(u,v) = \sum_{i=0}^{15} v_i B_i(u,v) \tag{28}$$

where

$$\{B_i(u,v)\}_{i=0}^{15} = \{\{B_i(u)B_j(v)\}_{j=0}^{3}\}_{i=0}^{3}$$

are the usual basis functions for uniform cubic B-spline surfaces. For extraordinary corner patches, such as the shaded patch of the initial control mesh shown in Fig. 21(b), the parametric form for surface evaluation is similar to Eq. (28) with another set of basis functions $\{\psi_i(u,v)\}_{i=0}^{K-1}$ as follows:

$$p(u,v) = \sum_{i=0}^{K-1} v_i \psi_i(u,v) \tag{29}$$

where $K=2n+8$ is the total number of control points for defining an extraordinary corner patch with valance n. The basis functions $\{\psi_i(u,v)\}_{i=0}^{K-1}$ of Eq. (29) can be derived following the eigen structure analysis of a subdivision matrix defined by the stencil shown in Fig. 21(b) and further details can be found in Refs. [29,49].

5. Subdivision surface fitting

In literature, one can also find various approaches for fitting subdivision surfaces to range or scanning data. Among others, Hoppe et al. [16] presented an approach for automatically fitting subdivision surfaces from a dense triangle mesh. Following the fitting criterion, the final fitted control mesh after two subdivisions will be the closest to the initial dense mesh, which provides sufficient approximation for practical applications. Both smooth and sharp models can be handled. This approach produces high quality visual models.

The method of Suzuki et al. [52] for subdivision surface fitting starts from an interactively defined initial control mesh. For each of the control vertices, the corresponding limit position is obtained from the initial dense mesh. The final positions of the control vertices are then inversely solved following the relationship between the control vertices and the corresponding limit positions. The fitted subdivision surface is checked against a predefined tolerance. In case of need, the topological structure of the control mesh is further subdivided and a refined mesh of limit positions is obtained. A new subdivision surface is then fitted from the corresponding refined limit positions. The procedure is repeated until the fitted subdivision surface meets the allowed tolerance bound. The fitting criterion ensures that the resulting subdivision surface interpolates the corresponding limit positions of the current control mesh. Since only a subset of vertices of the initial dense mesh is involved in the fitting procedure, the computing speed is extremely fast.

Ma and Zhao [28,29] also reported a parametrization-based approach for fitting Catmull–Clark subdivision surfaces. A network of global boundary curves is first interactively defined for topological modeling. A set of base surfaces is then defined from the topological model for sample data parametrization. A set of observation equations is obtained based on ordinary B-splines for regular surface patches and an evaluation scheme of Stam [49] for extraordinary surface patches. A Catmull–Clark surface is finally obtained through linear least squares fitting. The approach makes use of all known sample points and the fitting criterion ensures best fitting condition between the input data and the final fitted subdivision surface. Apart from the parametrization procedure, the fitting process alone is pretty fast.

In a recent paper, Ma et al. [30] proposed a direct method for subdivision surface fitting from a known dense triangle mesh. A feature- and topology-preserving mesh simplification algorithm is first used for topological modeling and a direct fitting approach is developed for subdivision surface fitting. For setting up the fitting equations, both subdivision rules and limit position evaluation masks are used. The final subdivision surface best fits a subset of vertices of the initial control mesh and is obtained through linear least squares fitting without any constraints. Sharp features are also preserved during the fitting procedure. Further work with improved fitting results can also be found in [24]. While only a modified Loop subdivision scheme [27] was discussed in these papers, the algorithm can be applied to all stationary subdivision schemes. The processing time is also extremely fast.

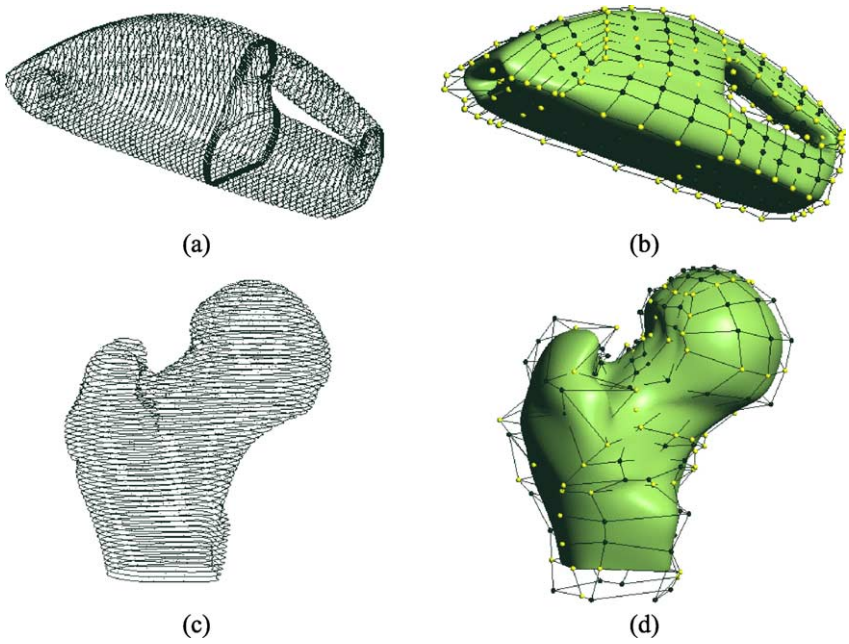

Fig. 22. A paramatrization-based approach for subdivision surface fitting [28,29]: (a) and (b) a vacuum cleaner model; (c) and (d) a piece of femur bone model; (a) and (c) original contours measured on a medical CT-scanner with extended interpolation points; (b) and (d) final fitted subdivision surface with control points.

All the above fitting approaches are built upon schemes for limit surface query, either at discrete positions [16,30, 52] or at arbitrary parameters [28,29]. In literature, one can also find schemes interpolating a set of surface limit positions with or without surface normal vectors instead of fitting conditions [15,34]. In theory, all interpolation schemes can be extended as a fitting scheme if the number of known surface conditions, such as limit positions, normal vectors and other constraints, is more than that of the unknown control vertices of the subdivision surface. Several authors [3,44,45] also explored reversal of Loop, Butterfly and the original Doo subdivisions through wavelets analysis and least squares fitting. Lee et al. [21] also proposed an approach for surface reconstruction, called a displaced subdivision surface, from an arbitrary triangle mesh with details. The displaced subdivision surface is defined as a smooth subdivision surface with a scalar-valued displacement map applied to the limit positions of a refined control mesh. The smooth subdivision surface was obtained through mesh simplification. Guskov et al. [13] also constructed a normal mesh with wavelets coefficients as hierarchical displacements applied to a multi-resolution mesh. The normal mesh can be considered as a kind of generalization of the displaced subdivision surfaces of Lee et al. [21]. One can also find an approach for adaptively fitting a Catmull–Clark subdivision surface to a given shape through a fast local adaptation procedure [26]. The fitting process starts from an initial approximate generic model defined as a subdivision surface of the same type.

Fig. 22 shows two fitting examples produced using the paramatrization based approach for subdivision surface fitting [28,29]. The original data for both of these models were measured using CT-scanners. Fig. 22(a) and (c) shows the original measured CT contours with superposed interpolation points. Fig. 22(b) and (d) show the final fitted Catmull–Clark surfaces. Further details regarding the fitting approach can be found in Refs. [28,29]. Fig. 23 shows two fitting examples produced using the direct approach for subdivision surface fitting [24,30]. Fig. 23(a) and (d) on the left are input triangle meshes. Fig. 23(b) and (e) in the middle are control meshes of the fitted Loop subdivision surface. Fig. 23(c) and (f) present the final fitted Loop subdivision surface. Further details regarding the fitting approach can be found in Refs. [24,30].

The above examples also demonstrate the modeling capability of subdivision surfaces. If one had used traditional B-splines, one would have had to maintain the continuity among individual surfaces, which is an extremely difficult task for today's CAD systems. Even if one can represent the entire model as a mosaic of B-spline surfaces with continuity conditions, it is still not possible to modify the surface by moving a control points near domain boundaries, or one breaks all the continuity conditions. With subdivision surfaces, however, the continuity conditions along all patch boundaries are automatically maintained. One can modify the shape by moving any of its control points, just like manipulating the control points of a single B-spline surface.

While many approaches have been reported so far, several other important areas may be further explored. On topological modeling, adaptive approaches and techniques for arbitrary mesh processing can be further studied.

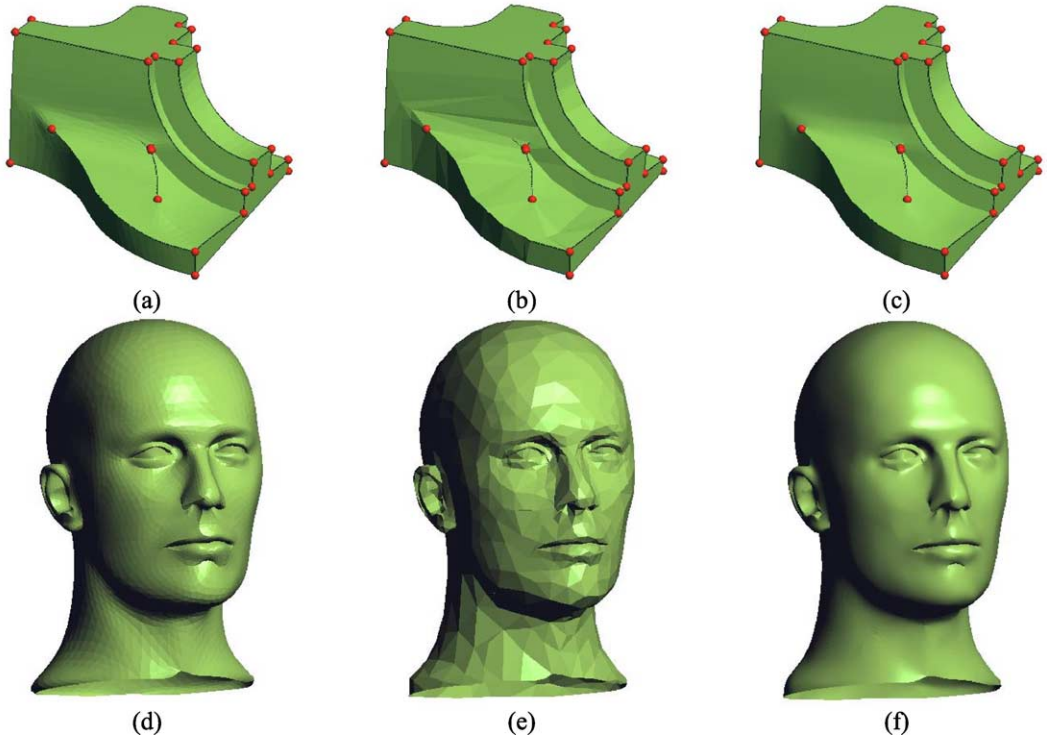

Fig. 23. A direct approach for automatic subdivision surface fitting [24,30]: (a)–(c) a test part with marked sharp features; (d)–(f) a mannequin model; (a) and (d) original triangle mesh; (b) and (e) control mesh of the fitted Loop subdivision surfaces; (c) and (f) final fitted Loop subdivision surfaces.

On stationary subdivision surface fitting, elaborated procedures may be developed to further handle fitting with various given constraints, such as known limit positions, local tangents and surface normal vectors. Local piecewise fitting procedures and adaptive approaches may also be further developed for parallel processing of extremely large surface meshes. Techniques for fitting non-stationary and other subdivision surfaces also need to be developed.

6. Other topics in subdivision surface modelling

During the past decade or so, subdivision surfaces have received extensive attention in free-form surface modelling, multi-resolution representation, and computer graphics. Families of new subdivision schemes were proposed, many new theoretical tools were developed, and various practical results were obtained. Recently, several other topics have also attracted enormous attention and there is a lot of space for further development in many other topics.

- *Unified subdivision schemes and standardization*: One of the topics addressed in recent years is the pursuit of unified subdivision schemes [31,35,50,55,57,62], an important step towards wide practical applications. Ultimately a further unified generalization like NURBS for the CAD and graphics community and further standardization are expected. Such a unified generalization should cover all what we can do with NURBS, including the exact definition of regular shapes such as sphere, cylinder, cone, and various general conical shapes and rotational geometry.
- *Continuity conditions at extraordinary corner positions*: Another topic is the lifting of continuity conditions at extraordinary corner positions in handling general degrees that should be the same as that for regular part of subdivision surfaces. While we are striving to seek subdivision schemes with small masks for simplicity, it should be acceptable as long as it is easy to implement, such as repeated averaging for generalizing high order B-splines [50,62].
- *Manipulation tools*: For wide practical use, advanced manipulation tools, such as trimming, intersection, offsetting, Boolean operations, visual effects must be developed. While there have be various attempts [4,25,33], there is significant space for further development in these areas.
- *Other topics*: Other important topics include further development in surface fitting and interpolation, faring subdivision surface generation, subdivision surface modeling from curve nets, mass property evaluation, geometry compression, interfacing issues and compatibility with existing parametric surface software, adaptive subdivision algorithms that lead to the same limit surface.

One may find further discussions in Refs. [42,43,56,61] regarding the above and some other topics on subdivision based modeling.

7. Conclusions

Similar to spline surfaces, subdivision surfaces are defined by a set of control points. Instead of explicit parametrization for defining B-spline surfaces, the parametrization of a subdivision surface is implicitly defined by its subdivision rules, i.e. topological rules for mesh refinement and geometric rules for computing vertices of refined meshes. While a subdivision surface is defined as the limit of recursive subdivision and refinement, algorithms for explicit parametric evaluation of subdivision surfaces in a single step may also be developed. Such a parametric evaluation has been reported for Catmull–Clark and Loop surfaces, but the technique can be applied to any stationary subdivision schemes whose parametric form exists for regular part of the surface. It might also be possible to develop an explicit form for parametric evaluation of other subdivision schemes through the analysis of the subdivision series for some other subdivision schemes. The most important merit of subdivision surfaces for the CAD and graphics community is the ability in handling control meshes of arbitrary topology. In addition, subdivision algorithms, if implemented properly, can form the basis for a wide range of extremely fast and robust interrogations. In literature, many subdivision schemes and elegant theoretical tools have been developed. Many other areas have been addressed and can be further developed, especially on unified subdivision schemes that is capable of generalizing the entire family of NURBS, the current de-facto standard for CAD and graphics. Many other algorithms for subdivision surface manipulation should also be developed for wide engineering applications.

Acknowledgements

The work presented in this paper was supported by City University of Hong Kong through a Strategic research Grant (7001296) and by the Research Grants Council of Hong Kong through a CERG research grant (CityU 1131/03E). The control mesh of the gun model shown in Fig. 19(c) was downloaded from http://www.elysium.co.jp/3dtiger/en/download/ Special thanks also go to N. Zhao, G. Li and Z. Wu for the implementation of several subdivision schemes at CityU.

References

[1] Ball AA, Storry DJT. Recursively generated B-spline surfaces. Proc CAD 1984;84:112–9.
[2] Ball AA, Storry DJT. Conditions for tangent plane continuity over recursively generated B-spline surfaces. ACM Trans Graph 1988; 7(2):83–102.
[3] Bartels R, Samavati F. Reverse subdivision rules: local linear conditions and observations on inner products. J Comput Appl Math 2000;119:29–67.
[4] Biermann H, Kristjansson D, Zorin D. Approximate Boolean operations on free-form solids. Proceedings of ACM SIGGRAPH computer graphics 2001 p. 185–94.
[5] Biermann H, Martin I, Zorin D, Bernardini F. Sharp features on multiresolution subdivision surfaces. Graph Models 2002;64(2): 61–77.
[6] Catmull E, Clark J. Recursively generated B-spline surfaces on arbitrary topological meshes. Comput Aided Des 1978;10:350–5.
[7] Chaikin G. An algorithm for high-speed curve generation. Comput Graph Image Process 1974;3:346–9.
[8] Daubechies I, Guskov I, Sweldens W. Regularity of irregular subdivision. Constr Approx 1999;15(3):381–426.
[9] DeRose T, Kass M, Truong T. Subdivision surfaces in character animation. In: Proceedings of ACM SIGGRAPH computer graphics, 1998. p. 85–94.
[10] Doo D, Sabin M. Behaviors of recursive division surfaces near extraordinary points. Comput Aided Des 1978;10:356–60.
[11] Dyn N, Levin D, Gregory JA. A butterfly subdivision scheme for surface interpolation with tension control. ACM Trans Graph 1990; 9(2):160–9.
[12] Dyn N. Subdivision schemes in computer aided geometric design. In: Light WA, editor. Advances in numerical analysis II, subdivision algorithms and radial functions. Oxford: Oxford University Press; 1992. p. 36–104.
[13] Guskov I, Vidimce K, Sweldens W, Schroder P. Normal meshes. Proceedings of ACM SIGGRAPH computer graphics July 2000 p. 95–102.
[14] Habib A, Warren J. Edge and vertex insertion for a class of C1 subdivision surfaces. Comput Aided Geom Des 1999;16: 223–47.
[15] Halstead M, Kass M, DeRose T. Efficient fair interpolation using Catmull–Clark surfaces. Proceedings of the ACM SIGGRAPH computer graphics 1993 p. 35–44.
[16] Hoppe H, DeRose T, Duchamp T, Halstead M, Jin H, McDonald J, Schweitzer J, Stuetzle W. Piecewise smooth surface reconstruction. Proceedings of the ACM SIGGRAPH computer graphics 1994 p. 295–302.
[17] Jena MK, Shunmugaraj P, Das PC. A non-stationary subdivision scheme for generalizing trigonometric spline surfaces to arbitrary meshes. Comput Aided Geom Des 2003;20:61–77.
[18] Kobbelt L. Interpolatory subdivision on open quadrilateral nets with arbitrary topology. Proceedings of eurographics 96, computer graphics forum 1996 p. 409–20.
[19] Kobbelt L. $\sqrt{3}$-subdivision. Proceedings of ACM SIGGRAPH computer graphics 2000 p. 103–12.
[20] Labisk U, Greiner G. Interpolatory $\sqrt{3}$-subdivision. Comput Graph Forum (EUROGRAPHICS 2000) 2000;19(3):131–8.
[21] Lee A, Moreton H, Hoppe H. Displaced subdivision surfaces. Proceedings of the ACM SIGGRAPH computer graphics July 2000 p. 85–94.
[22] Li G, Ma W, Bao H. $\sqrt{2}$ Subdivision for quadrilateral meshes. Vis Comput 2004;20(2–3):180–98.
[23] Li G, Ma W, Bao H. Interpolatory $\sqrt{2}$-subdivision surfaces. Proceedings of GMP : geometric modelling and processing—theory and applications. California: IEEE Computer Press; 2004 p. 185–94.
[24] Li G, Ma W, Bao H. A system for subdivision surface fitting. J Comput Aided Des Comput Graph 2004 [preprint].
[25] Litke N, Levin A, Schröder P. Trimming for subdivision surfaces. Comput Aided Geom Des 2001;18:463–81.
[26] Litke N, Levin A, Schröder P. Fitting subdivision surfaces. Proceedings of scientific visualization 2001 p. 319–24.
[27] Loop C, Smooth subdivision surfaces based on triangles, Master's Thesis, Department of Mathematics, University of Utah; 1987.

[28] Ma W, Zhao N. Catmull–Clark surface fitting for reverse engineering applications. Proceedings of GMP: geometric modelling and proccesing—theories and applications. California: IEEE Computer Society; 2000 p. 174–283.
[29] Ma W, Zhao N. Smooth multiple B-spline surface fitting with Catmull–Clark surfaces for extraordinary corner patches. Vis Comput 2002;18(7):415–36.
[30] Ma W, Ma X, Tso S-K, Pan ZG. A direct approach for subdivision surface fitting from a dense triangle mesh. Comput Aided Des 2004; 36(6):525–36.
[31] Morin G, Warren J, Weimer H. A subdivision scheme for surfaces of revolution. Comput Aided Geom Des 2001;18:483–502.
[32] Muller H, Jaeschke R. Adaptive subdivision curves and surfaces. Computer graphics International 1998, June 22—26, 1998, Hannover, Germany, IEEE Computer 1998 p. 48–58.
[33] Nasri AH. Interpolating meshes of boundary intersecting curves by subdivision surfaces. Visual Comput 2000;16(1):3–14.
[34] Nasri A, Sabin M. Taxonomy of interpolation constraints on recursive subdivision surfaces. Vis Comput J 2002;18(6):382–403.
[35] Oswald P, Schröder P. Composite primal/dual $\sqrt{3}$-subdivision schemes. Comput Aided Geom Des 2003;20(2):135–64.
[36] Peters P, Reif U. The simplest subdivision scheme for smoothing polyhedra. ACM Trans Graph 1997;16(4):420–31.
[37] Peters J, Reif U. Analysis of algorithms generalizing B-spline subdivision. SIAM J Numer Anal 1998;35(2):728–48.
[38] Prautzsch H. Smoothness of subdivision surfaces at extraordinary points. Adv Comp Math 1998;14:377–90.
[39] Prautzsch H, Umlauf G. A G2 subdivision algorithm. In: Farin G, Bieri H, Brunnett G, DeRose T, editors. Geometric modelling, computing suppl, vol. 13. Berlin: Springer; 1998. p. 217–24 p. 217–24.
[40] Reif U. A unified approach to subdivision algorithms near extraordinary vertices. Comput Aided Geom Des 1995;12(2): 153–74.
[41] Sabin MA. Cubic recursive division with bounded curvature. In: Laurent PJ, Mehaute A, Schu-maker LL, editors. Curves and surfaces. Academic Press; 1991 p. 411–4.
[42] Sabin MA. Subdivision surfaces. In: Farin GE, Hoschek J, Kim MS, editors. Handbook of computer aided geometric design. New York: North Holland; 2002. p. 309–25.
[43] Sabin MA. Recent progress in subdivision—a survey. In: Dodgson N, Floaterand MS, Sabin M, editors. Advances in multiresolution for geometric modelling. Berlin: Springer; 2004.
[44] Samavati F, Bartels R. Multiresolution curve and surface representation: reversing subdivision rules by least squares data fitting. Comput Graph Forum 1999;18:97–119.
[45] Samavati F, Mahdavi-Amiri N, Bartels R. Multiresolution surfaces having arbitrary topology by a reverse Doo subdivision method. Comput Graph Forum 2002;21:121–36.
[46] Schweitizer JE. Analysis and application of subdivision surfaces. PhD Thesis. Seattle, WA: University of Abhijit; 1996.
[47] Sederberg TW, Zheng J, Sewell D, Sabin M. Non-uniform recursive subdivision surfaces. Proceedings of the ACM SIGGRAPH computer graphics 1998 p. 387–94.
[48] Sovakar A, Kobbelt L. API design for adaptive subdivision schemes. Comput Graph 2004;24:67–72.
[49] Stam J. Exact evaluation of Catmull–Clark subdivision surfaces at arbitrary parameter values. Proceedings of the ACM SIGGRAPH computer graphics 1998 p. 395–404.
[50] Stam J. On subdivision schemes generalizing uniform B-spline surfaces of arbitrary degree. Comput Aided Geom Des 2001;18(5): 383–96.
[51] Stam J, Loop C. Quad/triangle subdivision. Comput Graph Forum 2003;22(1):1–7.
[52] Suzuki H, Takeuchi S, Kanai T, Kimura F. Subdivision surface fitting to a range points. Proceedings of the seventh Pacific graphics international conference 1999 p. 158–67.
[53] Umlauf G. Analyzing the characteristic map of triangular subdivision schemes. Constr Approx 2000;16(1):145–55.
[54] Velho L, Zorin D. 4–8 Subdivision. Comput Aided Geom Des, Spec Issue Subdivision Tech 2001;18(5):397–427.
[55] Warren J, Schaefer S. A factored approach to subdivision surfaces. Comput Graph Appl 2004;24(3):74–81.
[56] Warren J, Weimer H. Subdivision methods for geometric design. Subdivision methods for geometric design, a constructive approach. Boston: Morgan Kaufmann Publishers; 2002.
[57] Wu X, Thompson D, Machiraju R. A generalized corner-cutting subdivision scheme. http://www.cse.Ohio-state.edu/(raghu/Papers/cagd_wu.pdf; 2002.
[58] Zorin D. Smoothness of stationary subdivision on irregular meshes. Constr Approx 2000;16(3):359–97.
[59] Zorin D. A method for analysis of C1-continuity of subdivision surfaces, SIAM. J Numer Anal 2000;37(5):1677–708.
[60] Zorin D, Schröder P, Sweldens W. Interpolating subdivision for meshes with arbitrary topology. Proceedings of the ACM SIGGRAPH computer graphics 1996 p. 189–92.
[61] Zorin D, Schröder P. Subdivision for modeling and animation. ACM SIGGRAPH Course Notes, New Orleans, July 23–28 2000.
[62] Zorin D, Schröder P. A unified framework for primal/dual quadrilateral subdivision scheme. Comput Aided Geom Des 2001; 18(5):429–54.

Weiyin Ma is an Associate Professor in manufacturing engineering at the City University of Hong Kong (CityU). He lectures in the areas of geometric modeling, CAD/CAM and rapid prototyping. His present research interests include computer aided geometric design, CAD/CAM, virtual design and virtual manufacturing, rapid prototyping and reverse engineering. Prior to joining CityU, he worked as a research fellow at Materialise N.V., a rapid prototyping firm in Belgium. He also worked in the Department of Mechanical Engineering of Katholieke Universiteit Leuven (K.U. Leuven), Belgium, and the Department of Space Vehicle Engineering of East China Institute of Technology (ECIT), China. He obtained a BSc in 1982 and an MSc in 1985 from ECIT, an MEng in 1989 and a PhD in 1994 from K.U. Leuven.